Near-Threshold High-Order Harmonic Spectroscopy with Aligned Molecules

H. Soifer,[1] P. Botheron,[2] D. Shafir,[1] A. Diner,[1] O. Raz,[1] B. D. Bruner,[1] Y. Mairesse,[2] B. Pons,[2] and N. Dudovich[1]

[1]*Department of Physics of Complex Systems, Weizmann Institute of Science, 76100 Rehovot, Israel*
[2]*CELIA, Université de Bordeaux I-CNRS-CEA, 351 Cours de la Libération, 33405 Talence, France*

We study high-order harmonic generation in aligned molecules close to the ionization threshold. Two distinct contributions to the harmonic signal are observed, which show very different responses to molecular alignment and ellipticity of the driving field. We perform a classical electron trajectory analysis, taking into account the significant influence of the Coulomb potential on the strong-field-driven electron dynamics. The two contributions are related to primary ionization and excitation processes, offering a deeper understanding of the origin of high harmonics near the ionization threshold. This Letter shows that high-harmonic spectroscopy can be extended to the near-threshold spectral range, which is in general spectroscopically rich.

High-harmonic generation (HHG) in strong-field light-matter interactions is generally understood in terms of a three-step process. An electron is removed from the target, accelerated, and driven back to its parent ion by the laser field. Finally, it recombines into the bound state, and emits a high-harmonic photon [1]. This process has been extensively studied for harmonics with energies higher than the ionization threshold (I_p), corresponding to frequencies in the extreme ultraviolet range. In this Letter, we focus on the intricate region close to the threshold and use aligned molecules to elicit the dynamics of near-threshold HHG.

The spectral region near the ionization threshold is, in general, spectroscopically very rich. In this respect, using near-threshold harmonic spectroscopy to probe specific structures such as resonances is an appealing alternative to standard photoionization spectroscopy. It could help uncover nontrivial attosecond dynamics occurring near the threshold, such as excitation of electronic wave packets or ionization via resonant states [2,3]. However, the extension of high-harmonic spectroscopy to the threshold region requires a detailed knowledge of the underlying HHG mechanisms in this specific regime.

Furthermore, high-harmonic spectroscopy is being used in a growing number of experiments to measure the structure and dynamics of small atomic and molecular systems with unprecedented subfemtosecond and angstrom resolution [4–9]. As we move to more complex molecular structures, several orbitals contribute to the laser-target interaction and nontrivial hole dynamics are induced. Because of the contribution of multiple orbitals, there is no clear distinction between near- and above-threshold harmonics. The ability to identify the different processes in this regime is an essential step towards decoupling and identifying the contributions from the various orbitals.

Above the ionization threshold, the intuitive three-step model is qualitatively confirmed and quantitatively reinforced by the strong-field approximation (SFA) [10]. In this

model, a photon at frequency ω is emitted in the energy range $I_p \lesssim \hbar\omega \lesssim I_p + 3.17U_p$, where I_p is the ionization potential and U_p the ponderomotive energy. In the SFA, the free electron is controlled by the strong laser, whereas the Coulomb potential is neglected. The SFA predicts many of the fundamental characteristics of HHG, in particular, the fact that each harmonic mainly stems from two electronic pathways, commonly referred to as "short" and "long" trajectories [11]. However, the SFA is not accurate as we approach the ionization threshold, where the Coulomb force cannot be neglected [12].

There has recently been increased interest in the near-threshold regime [13–15]. Yost *et al.* have considered the generation of harmonics below the ionization threshold in xenon atoms [13]. In conjunction with measurements of harmonic yields as functions of the laser intensity, they solved the time-dependent Schrödinger equation and identified two distinct contributions to below-threshold harmonics, with different intensity-dependent phases. The contribution with the highest intensity dependence of the phase was attributed to long electron trajectories, whereas the second contribution, with smaller intensity dependence, was related to primary multiphoton processes. Hostetter *et al.* [15] supported this observation from a semiclassical point of view.

How can we directly and experimentally distinguish between the different HHG processes in the vicinity of the ionization threshold? There are two important knobs that can be used to manipulate the HHG process. The first knob is related to the structure of the bound state and can be manipulated by producing harmonics from aligned molecules. The second is related to the free electron dynamics and can be tuned by controlling the laser ellipticity. Here we combine the two knobs, using extensively studied N_2 and O_2 molecules, and manipulate both the target structure, through alignment, and the laser field, which guides the free electron wave packet. Such a manipulation

is applied to elicit the dynamical features of threshold HHG. In addition, we perform a theoretical analysis in terms of classical electron trajectories, which yields an intuitive picture of the interaction and improves our understanding of the underlying mechanisms.

The experiment is composed of two parts. We control the molecules using a pump-probe setup in which the pump creates rotational wave packets and the probe generates the harmonic signal [16]. Once the molecular axis is fixed we manipulate the free electron's dynamics by scanning the ellipticity of the probe beam. High harmonics are generated with an 800-nm, 30-fs, 1-KHz laser beam, focused into a pulsed gas jet at $\sim 1.5 \times 10^{14}$ W/cm^2 intensity. As a pump we use part of the 800-nm beam, which we focus at a few 10^{13} W/cm^2 in the jet. The probe ellipticity ϵ is controlled by rotating a half wave plate in front of a fixed quarter wave plate in order to keep the main axis of the polarization ellipse fixed. ϵ is defined through $F(t) = F_0 \cos(\omega t)\hat{x} + i\epsilon F_0 \sin(\omega t)\hat{y}$, and the total intensity $|F|^2$ is kept constant throughout the experiment. We perform this scan for alignment angles of 0° and 90°. The harmonics are dispersed by a 1200 mm^{-1} grating and imaged on microchannel plates. The cylindrical geometry of the grating, combined with an optimized adjustment of the position of the gas jet with respect to the laser focus, enables us to discriminate between short and long trajectories, spectrally and spatially, in both below- and above-threshold regimes [13,17]. In the following, we will focus on the spectral range in the vicinity of the ionization potentials of N$_2$ and O$_2$, which, respectively, correspond to $10.05\omega_0$ and $8.78\omega_0$, where ω_0 is the fundamental laser frequency.

Figure 1 shows the harmonic signal as a function of the laser ellipticity for O$_2$ molecules for alignment angles of 0° (left) and 90° (right). Long trajectories were measured down to harmonic 11. As we increase the laser ellipticity, all the long trajectories' signals (bottom panels) decrease significantly. Such a response has been explained by the SFA for above-threshold harmonics [18]: the ellipticity of
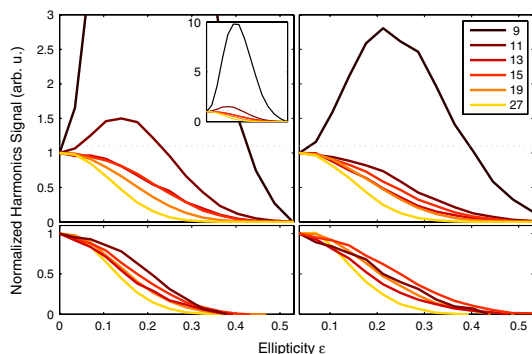
the driving field induces a lateral shift of the free electron wave packet, and therefore reduces the recombination probability. In the vicinity of the ionization threshold, we observe a similar effect.

As we switch from long to short trajectories, a striking difference appears. For an alignment angle of 0°, harmonics 9 and 11 increase as a function of the ellipticity and reach a maximum at $\epsilon \sim 0.2$ and 0.15, respectively. The signal at this point is enhanced by a factor of 9.8 ± 0.7 for the 9th harmonic and by 1.5 ± 0.1 for the 11th harmonic. A similar effect is observed for an alignment angle of 90°, but only for the 9th harmonic (2.7 ± 0.2). When the intensity I is slightly increased (from ~ 1.6 to $\sim 1.8 \times 10^{14}$ W/cm^2) this enhancement is observed in an additional harmonic—13 and 11 for 0° and 90°, respectively. Well above the ionization threshold, all short trajectories' responses exhibit the usual decaying rate, regardless of the intensity.

Repeating the experiment with N$_2$ molecules, no anomalous responses are observed. All harmonic orders decay smoothly as a function of ϵ, exhibiting similar decay rates for both short and long trajectories (not shown). So, while all long trajectories follow the expected ellipticity response as predicted by the intuitive three-step model, the reactions of near-threshold short trajectories are system dependent and highly selective. The observed enhancements at $\epsilon \neq 0$ cannot be related to the structure of the ground molecular orbital, and related interference processes at the time of recombination [19], since these latter would affect both short and long trajectories. We shall return to this point later, in the context of our theoretical analysis.

An additional difference between short and long trajectories in N$_2$ molecules near I_p is observed when the pump-probe delay is scanned using linearly polarized beams. Figure 2 shows the results of our pump-probe scans around the half-revival of N$_2$ [16], for both short and long trajectories. As observed in previous experiments, the total harmonic signal peaks at a delay of 4.1 ps, when the molecules are aligned along the polarization axis of the pump pulse, and has a minimum at 4.3 ps, when the
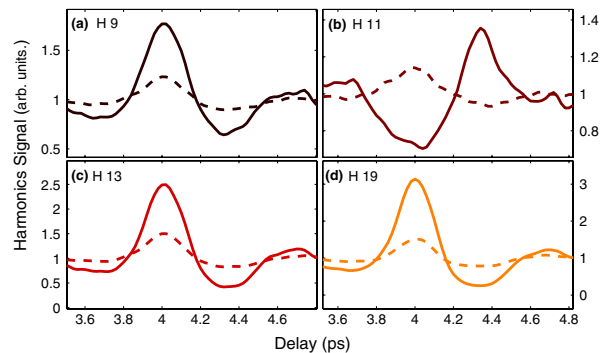
FIG. 1 (color online). Harmonic yields in O$_2$ aligned at 0° (left) and 90° (right), for long (bottom) and short (top) trajectories, as functions of the ellipticity ϵ of the probe pulse. The signal from each harmonic is normalized to its value at $\epsilon = 0$. The inset shows the full scale of the increase in harmonic 9.

FIG. 2 (color online). Normalized harmonic yields in rotationally excited N$_2$ for harmonics 9–13,19, as a function of the pump-probe delay. The solid lines and dashed lines correspond to the short and long trajectories, respectively.

molecules are antialigned [see Figs. 2(a), 2(c), and 2(d) for harmonics 9, 13, and 19]. Long trajectories were measured down to the 9th harmonic, with the typical revival structure (dashed lines in Fig. 2). However, the 11th harmonic has surprising features. Whereas the long trajectory exhibits the typical revival shape, with contrast $\frac{max - min}{max + min} = 0.10 \pm 0.03$, the short one (solid line) displays an inverted structure ($\frac{max - min}{max + min} = 0.35 \pm 0.04$). In order to verify that the inversion effect we observe does not depend on propagation, we performed a systematic study by varying the gas pressure by 1 order of magnitude and found similar results. An intensity scan from 1 to 2×10^{14} W/cm^2 also shows the robustness of this effect. Only below 1.2×10^{14} W/cm^2 does the inversion of harmonic 11 disappear.

Both experiments—the ellipticity and revival scans—indicate that threshold harmonics are generated by two completely different processes. Whereas the long trajectories behave as higher harmonic orders and therefore seem to be generated according to the standard three-step model, it is clear that the short trajectories originate from a different mechanism. How can threshold harmonics be explained in the framework of classical trajectories? What breaks the symmetry between the two families of electron trajectories?

In order to answer these fundamental questions, we have performed statistical classical trajectory Monte Carlo (CTMC) calculations [20] that treat the laser V_F and Coulomb V_C potentials on the same footing. We consider the prototypical N$_2$ system described in terms of a one-dimensional scaled hydrogen atom with an effective nuclear charge Z_e such that $Z_e = \sqrt{2I_p}$. The CTMC procedure employs an N-point discrete representation of the phase-space distribution, $\varrho(x, p, t) = \frac{1}{N} \times \sum_{j=1}^{N} \delta(x - x_j(t))\delta(p - p_j(t))$, in terms of N noninteracting trajectories $\{x_j(t), p_j(t)\}_{j=1,...,N}$. The initial condition, $\varrho(x, p, t = 0)$, consists of the Wigner phase-space distribution associated with the fundamental classical energy bin, as detailed in [20].

The CTMC picture of HHG is obtained by considering an instantaneous recombination to the ground state at time t' whenever a trajectory with energy $E(t') = p(t')^2/2 + V_C(t')$ returns to $x(t') = 0$ after having been ionized at time t''. Such a process is accompanied by the emission of a photon with energy $E(t') + I_p$. Figure 3 presents the harmonic order of the photon emitted upon recombination as a function of time t' of emission. Our CTMC results are compared to their SFA counterparts. For above-threshold emission, CTMC and SFA results are in good agreement. In contrast to the SFA, the CTMC method yields long trajectories for below-threshold harmonics; in the (t', H) plane of Fig. 3, these trajectories appear as continuations of the above-threshold ones below I_p.

To illustrate how these trajectories succeed in returning to the ion with $E(t') < 0$, we present in Fig. 4 the temporal evolution of the electron position $x(t)$ and of the energy
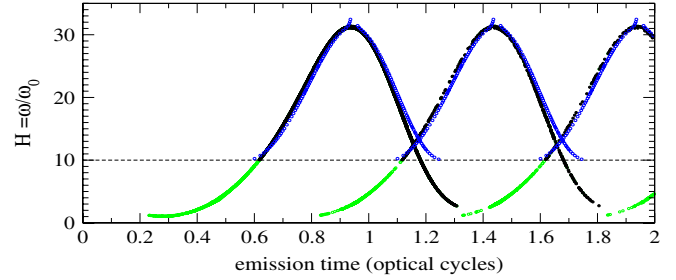

FIG. 3 (color online).   Calculated harmonic order as a function of time of emission t', for N$_2$ embedded in a two-cycle field with $\lambda = 800$ nm and $I = 1.5 10^{14}$ W/cm^2. The empty (blue) circles correspond to SFA calculations, whereas dark (black) and light (green) dots, respectively, represent harmonics stemming from ionizing and excitation trajectories, in the framework of CTMC-Wigner calculations.

$E(t) = p(t)^2/2 + V_C(t)$, for some typical long trajectories. Ionization occurs at $t'' \sim 0.3T_0$, where T_0 is the laser period, soon after the field maximum. At this time, the dispersion of the free wave packet in coordinate space, although small, is sufficient to allow the subsequent differentiation of the trajectories in the combined laser and Coulomb fields. The electron returns to the origin $x = 0$ at $0.95T_0 \lesssim t'' \lesssim 1.3T_0$. Earlier electrons emit higher harmonics. At the time of recollision, the laser force $-F(t)$ acting on the electron is in the opposite direction to the Coulomb force [13]. Negative energy $E(t')$ is enabled for those later trajectories that recombine at $t' \sim 1.25T_0$, where $p^2(t')/2 + V_C(t') < 0$. Our CTMC model thus shows clear continuity between above- and below-threshold harmonics for the long trajectories. All of them obey the standard three-step process and therefore have similar responses to ellipticity and revival scans.
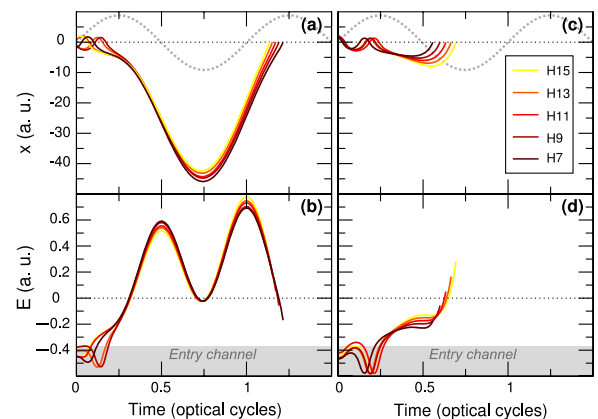

FIG. 4 (color online).   Calculated electron position x (a),(c) and energy E (b),(d) as functions of time t, for some short (right column) and long (left column) trajectories of Fig. 3. The dotted line in (a) and (c) represents the evolution of the electric field $F(t)$.

When the same analysis is applied to short trajectories, no below-threshold harmonics appear (see Fig. 3). We thus modify our model by relaxing the condition regarding ionization: we only require the trajectory to leave the fundamental classical energy bin before it returns back to $x = 0$, but we do not require it to be ionized (see Fig. 4). In other words, we allow excitation pathways to contribute to HHG. The results corresponding to this new criterion are included in Fig. 3; below-threshold short trajectories emerge, which is consistent with our experimental observations. They appear as the continuation below I_p of the above-threshold short trajectories. Their temporal evolution is illustrated in Figs. 4(c) and 4(d). The short trajectories corresponding to $\omega \gtrsim I_p$ are ionized shortly before recombination, whereas for below-threshold HHG, the trajectories recombine before ionization, with $E(t') < 0$. Inversely to what occurs for long trajectories, earlier electrons emit lower harmonics. Clearly, part of the below-threshold HHG signal stems from excitation processes, which are classically described in terms of short trajectories. Interestingly, a Bohmian description of the interaction yields quantum trajectories that nicely match, in both position and energy scales, the short CTMC trajectories [21]. Those trajectories do not involve tunnel ionization, in agreement with the semiclassical calculations of [15], and therefore are beyond the scope of the conventional three-step model.

We can now reinterpret the experimental observations concerning short trajectory below-threshold harmonics in light of their excitation origin. With respect to the ellipticity dependence observed in Fig. 1, a description of excitation in terms of a nonresonant absorption of H photons leads to harmonic yields that smoothly decrease as ϵ increases, in agreement with the N_2 shapes. This regular behavior is modified if intermediate resonances come into play during the multiphoton absorption, as shown in [22] for atomic targets. As ϵ increases, the interplay between the decreasing linear and increasing circular field components then yields ϵ responses similar to those of $H = 9$–13 in O_2. Obviously, the occurrence of resonances depends not only on the target considered, but also on the alignment angle that determines the allowed symmetry of the intermediate excited states. Resonantly enhanced excitation may also induce the inversion of revival structures. Depending on the symmetries of the intermediate states involved in the multiphotonic pathway, the harmonic strength can be maximal for a different molecular alignment than in the conventional three-step process involving tunneling. Finally, it is well known in strong-field physics that the ionization threshold of a target embedded in an intense laser field is subject to an ac-Stark ascending shift proportional to F^2. In this respect, the short trajectories associated with harmonic orders close to the unperturbed I_p recombine at time t', where $F(t') \neq 0$. Therefore, harmonic orders $H \gtrsim I_p/\omega_0$, which belong to above-threshold HHG at low I, fall down in the below-threshold regime as I increases. Accordingly, we understand the appearance of additional anomalous responses to ϵ in O_2 as I increases, and why the inversion of harmonic 11 disappeared in N_2 for $I \leq 1.2 \times 10^{14}$ W/cm^2, where $H = 11$ then effectively corresponds to above-threshold HHG.

To sum up, our joint experimental and theoretical study of harmonic generation in aligned N_2 and O_2 has allowed us to observe and explain, unambiguously, two main contributions to near-threshold HHG. The long electron trajectories belong to the three-step model and encode the structural information in the same way as in conventional high-harmonic spectroscopy. The short trajectories stem from multiphoton-driven pathways, and can be used to reveal complementary information on excited states of the molecule. The ellipticity and alignment responses of the short trajectory signal will provide information on the symmetry and dynamics of the intermediate states involved in the multiphoton process. This approach adds to the ability of HHG spectroscopy to follow a molecular orbital during chemical dynamics [23]. Since this method is extremely sensitive to the location of I_p, it is possible to probe changes in the threshold itself during chemical processes. Thus, our study is an integral part of the ongoing effort to resolve the structure as well as the dynamics of molecular orbitals.

[1] P. B. Corkum, Phys. Rev. Lett. **71**, 1994 (1993).
[2] S. Haessler et al., Phys. Rev. A **80**, 011404 (2009).
[3] J. Mauritsson et al., Phys. Rev. Lett. **105**, 053001 (2010).
[4] J. Itatani et al., Nature (London) **432**, 867 (2004).
[5] J. Marangos et al., Phys. Chem. Chem. Phys. **10**, 35 (2008).
[6] D. Shafir et al., Nature Phys. **5**, 412 (2009).
[7] O. Smirnova et al., Nature (London) **460**, 972 (2009).
[8] B. K. McFarland et al., Science **322**, 1232 (2008).
[9] S. Haessler et al. Nature Phys. **6**, 200 (2010).
[10] M. Lewenstein et al., Phys. Rev. A **49**, 2117 (1994).
[11] P. Antoine, A. L'Huillier, and M. Lewenstein, Phys. Rev. Lett. **77**, 1234 (1996).
[12] O. Smirnova, M. Spanner, and M. Y. Ivanov, Phys. Rev. A **77**, 033407 (2008).
[13] D. C. Yost et al., Nature Phys. **5**, 815 (2009).
[14] E. P. Power et al., Nat. Photon. **4**, 352 (2010).
[15] J. A. Hostetter et al., Phys. Rev. A **82**, 023401 (2010).
[16] J. Itatani et al., Phys. Rev. Lett. **94**, 123902 (2005).
[17] P. Salières, A. L'Huillier, and M. Lewenstein, Phys. Rev. Lett. **74**, 3776 (1995).
[18] P. Antoine et al., Phys. Rev. A **53**, 1725 (1996).
[19] T. Kanai, S. Minemoto, and H. Sakai, Phys. Rev. Lett. **98**, 053002 (2007).
[20] P. Botheron and B. Pons, Phys. Rev. A **80**, 023402 (2009).
[21] P. Botheron and B. Pons, Phys. Rev. A **82**, 021404(R) (2010).
[22] K. Miyazaki and H. Takada, Phys. Rev. A **52**, 3007 (1995).
[23] H. J. Wörner et al., Nature (London) **466**, 604 (2010).